CHAPTER 6

The use of SS biochar for Cr(VI) uptake and statistical optimization via RSM

6.1 Introduction

The rapid unstoppable growth in the world population demands more energy, and thus, it has accelerated the industrialization and urbanization. This growth in the industrial sector has led to the shortage as well as pollution of the water resources. Industrial wastewater is the major source of heavy metals (specific gravity > 5) like Cu, Zn, Pb, Cr, Fe, Cd, Ni, Hg, etc. to these water resources (Sundararaju et al., 2020). This wastewater, when get mixed with these natural water resources, makes it hazardous and toxic to the aquatic animals, plants and human being as well. Cr, one of the toxic heavy metal, is being discharged to water bodies from various industries like electroplating, petroleum refining, leather tanning, textile, pulp and paper industries etc. (Cheng et al., 2020). The discharge of Cr by these industries creates severe environmental pollution as well as health-related problems due to its non-biodegradable and bioaccumulative nature. From the eco-toxicological perspective, Cr is one of the most toxic element which lies in the list of top 16 toxic heavy metals that are injurious to human health (Gardea-Torresdey et al., 2000).

In water, Cr exists mainly in two different oxidation states i.e. trivalent (Cr(III)) and

hexavalent (Cr(VI)). The different oxidation states of Cr exhibit its different characteristics in terms of its impact on human or other living creatures. Of its two oxidation states, Cr(III) is an essential metal nutrient required by human beings for the metabolism of glucose as well as to potentiate insulin (Vinodhini and Das, 2009). On the contrary, Cr(VI) is highly carcinogenic and toxic around more than 500 times to Cr(III). Because of its high carcinogenicity, mutagenicity, toxicity and teratogenicity, Cr(VI) can lead to a lot of serious health problems on its exposure. High Cr(VI) concentration and its long-term exposure may damage lungs, liver and kidney. Various diseases that may occur due to its contact include Alzheimer's disease, dermatitis, genetic disorder, skin rashes, weakening of immune system etc. and even cancer (Kapur and Mondal, 2013; Rathore et al., 2017). According to WHO (World Health Organisation), the permissible limit for Cr(VI) concentration in drinking water is 0.05 mg/L. Therefore, due to its various harmful effects and high toxicity, wastewater containing Cr(VI) must be treated strictly prior to its disposal to water or soil environment.

Over the years, various physical and chemicals methods like chemical precipitation, flocculation-coagulation (Chang and Wang, 2007), solvent extraction, membrane separation, ion exchange, ultrafiltration, reverse osmosis (Fu and Wang, 2011) etc. have been useful for the eradication of Cr(VI) from wastewater. However, each method has its own advantages as well as certain limitations. These methods are quite expensive, energy-intensive, and less effective to bring down the Cr(VI) concentration to the permissible range and also some of the methods generate toxic sludge that too requires treatment before disposal. Also, these methods are not effective for the treatment metals with low concentrations (Abbas et al., 2014). Adsorption is a surface phenomenon that is characterized by good surface interaction, surface area as well as porosity. It is easy to

perform, low cost, higher efficiency and even metals with lower concentrations can be adsorbed.

Biochar is a very useful and promising adsorbent because of its low cost and excellent adsorption effect (Zhang et al., 2017). It is produced from pyrolysis of biomass like agricultural or municipal waste etc. pyrolysis of biomass not only helps in utilizing the waste biomass but also provides positive response to the environmental problems. Many researchers have reported regarding the better adsorption capacity of biochar in treating wastewater. In the past, biochar from various biomasses have been used for the treatment of heavy metals and biochar obtained from some of them like pine-apple peel (Wang et al., 2016), oleaster seed and cherry stone (Kahraman and Pehlivan, 2017), corn cob (Gupta et al., 2018) etc. were employed for Cr(VI) adsorption. Especially for treating micro pollutants biochar is more environmentally beneficial as compared to activated carbon derived from coal powder (Choudhary and Paul, 2018).

So based on the aforesaid facts, the study of Cr(VI) adsorption using biochar derived from SS was done. The effect of process variables solution pH, time, temperature, and adsorbent dose/Cr(VI) concentration ratio on Cr(VI) removal was investigated. The process has been optimized using RSM through BBD to maximize the removal of Cr(VI) as well as to study the interaction effect of process parameters. The concerned kinetic models, isotherm models, the thermodynamic properties and mass transfer studies were analyzed and calculated. The possible adsorption mechanism for Cr(VI) onto SS biochar has been proposed, which was affirmed by FTIR, X-ray photoelectron spectra (XPS) and SEM-EDX analyses. The adsorbent was further regenerated and reused in the adsorption process to portray its reusability. Such detailed study describing the efficacy of SS biochar for Cr(VI) adsorption along with the combined interaction effect of process variables in maximizing Cr(VI) removal has not been discussed earlier.

6.2 Experimental

6.2.1 Adsorbent

The adsorbent used in the current study was biochar obtained as by-product after pyrolysis of SS as discussed in our previous chapter 5. The biochar collected was rinsed twice with double distilled water to eradicate any contamination if it had onto its surface and then dried in the sunlight for 1 day. Further, biochar was dehydrated in the air oven at 105 °C to make its surface active for further experiments. It was finally stored in vacuum desiccators for its use in adsorption process.

6.2.2 Reagent preparation

All the reagents and chemicals used for the experiments were of analytical grade and the solutions were prepared with double distilled water (DDW). 1,5-diphenyl carbazide (DPC) was procured from C.D.H. Ltd. (New Delhi, India). Potassium dichromate ($K_2Cr_2O_7$), potassium nitrate (KNO_3) and 97 % pure sulphuric acid were obtained from Fischer Scientific, Qualigens chemicals Ltd., India. Sodium hydroxide pellets and hydrochloric acid were obtained from S.D.F Chem Ltd. (India). 2.8287 g of $K_2Cr_2O_7$ powder was dissolved in 1000 mL of DDW to prepare Cr(VI) stock solution. For DPC solution, 250 mg of DPC was dissolved in 50 mL of acetone.

6.2.3 Analytical instruments/equipments and methods used

The instruments and techniques used for the characterization of adsorbents before and after adsorption were similar as discussed in section 4.2.3. In addition, to investigate the presence the of Cr on biochar surface after adsorption as well as to study the change in oxidation state of Cr the XPS (Kratos A. Ltd., U.K.) analysis of the adsorbent was done. A digital pH meter (Systronics, Ahmedabad, India) was employed to measure the pH of the solution. A water bath shaker (Calton, NSW/133, New Delhi, India) equipped with PID controller was employed for shaking and sustaining the necessary temperature for

the batch experiments. The detection of Cr in the standard and treated samples was done via UV-visible spectrophotometer (Elico, SL-159, India) at the wavelength of 540 nm.

6.2.4 Adsorption experimental procedure

Experiments were performed in batch operation using biochar as adsorbent to study its effectiveness in Cr(VI) elimination from aqueous phase. Dilution of stock solution was done with DDW to acquire the solution of requisite concentration for different experimental runs. The experiments were executed at room temperature of 30 ± 1 °C and rotation speed of 150 rpm except for the experiments of effect of temperature. The parameters varied are pH (2-12), temperature (30 - 40 °C), contact time (0-90 min), initial metal ion concentration (30-100 mg/L), and dose/ concentration ratio (16.67-200). The adsorbent particle size was kept constant and it was in between 0.177-0.250 mm (geometric mean = 0.2103 mm). 0.1 M NaOH and 0.1 M HCl were used to bring the pH of the liquid at its required value. The experiments were executed in conical flasks of 100 mL where 50 mL of solution was taken with required amount of adsorbent. It was then fixed in conical channels inside the water bath shaker and shaken continuously till equilibrium time. After that, flasks were brought out from the shaker at required time gap and the liquid was filtered (Whatman filter paper-42). The supernatant liquid was then analyzed to calculate the final Cr(VI) concentration after adsorption according to the techniques for assessment of water and wastewater, AWWA, APHA, WPCF (1975) by means of UV-visible spectrophometer at wavelength of 540 nm. The % Cr(VI) removal and equilibrium adsorption capacity of adsorbent were obtained following eq. 6.1 and 6.2, respectively.

$$\textbf{\% Cr(VI) removal} = \left(\frac{C_o - C_t}{C_o}\right) \times 100 \qquad (6.1)$$

$$\textbf{Equilibrium adsorption capacity } (q_e) = \left(\frac{C_o - C_e}{W}\right) \times V \qquad (6.2)$$

Where, C_0, C_t and C_e are concentrations (mg/L) of Cr(VI) at initial, any time t and at equilibrium, V is the liquid volume in L, W is the adsorbent weight in mg and equilibrium adsorption capacity is denoted by q_e in mg/g. All the experiments were performed in triplicate and average value has been reported.

6.2.5 Optimization using RSM

The Design Expert software with BBD was used to optimize the process variables in maximizing the % Cr(VI) removal. Three significant variables that affect the % removal were varied i.e. Solution pH, temperature (°C) and dose/Cr(VI) concentration (mg/mg). The required number of experimental runs in BBD is set by the equation $N = k^2 + k + N_0$, where, N_0 and k represents repeated central experiment and factor number, respectively. Based on 3 (-1, 0, +1) factors, total 17 experiments were performed including 5 central experiments. The different BBD level and experimental parameters are presented in Table 6.1.

Table 6.1 Range of independent process variables and experimental levels

Process variables	**Experiment levels**		
	-1	**0**	**1**
pH	2	2.5	3
Temperature (°C)	30	35	40
Dose/Cr(VI) concentration (mg/mg)	100	133.33	166.37

The results were further assessed by ANOVA (analysis of variance), R^2 (co-efficient of determination) and 3 D plots based on interaction of parameters. The experimental data was fitted to a second order non-linear quadratic equation given below and co-efficient was determined.

$$Y_1 = \beta_0 + \sum \beta_i X_i + \sum \beta_{ii} X^2_i + \sum \beta_{ij} X_i X_j \quad (6.3)$$

Where, Y_1 is the approximate response (% removal), β_0 is the unvarying regression co-efficient β_i, β_{ii} and β_{ij} are the coefficients of linear, quadratic and interactive terms. X_i and X_j are the coded values for independent variables.

6.3 Results and Discussions

6.3.1 Physicochemical characteristics of adsorbent

6.3.1.1 BET and point of zero charge (pH_{zpc}) analysis

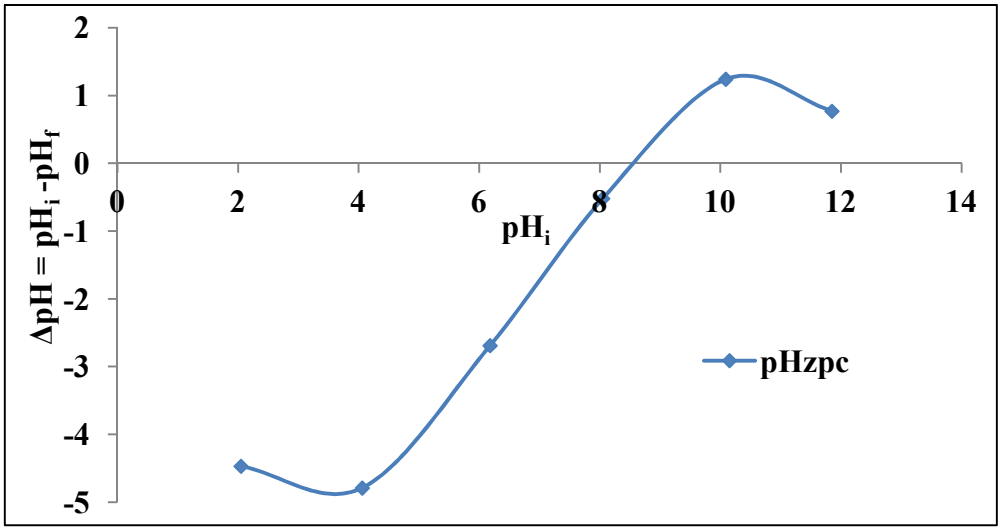

Fig. 6.1 pH_{zpc} of the biochar

The BET surface area of this biochar is discussed in section 5.3.4.1. pH_{zpc} is another property that helps in understanding the adsorption reaction mechanism and it was obtained by solid addition method (Rathore et al., 2017). The uptake of cations is preferred at pH > pH_{zpc} whereas anions adsorption is preferential at pH < pH_{zpc}. The pH_{zpc} for the biochar was 8.4 as shown in Fig. 6.1 where pH_i, pH_f and ΔpH denote initial, final (48 h later after the addition of biochar to the solution) and change in pH of

the liquid. The result shows that towards lower pH, the biochar surface has high positive indict with the affinity to adsorb negatively charged chromate ions from the solution.

6.3.1.2 XRD analysis

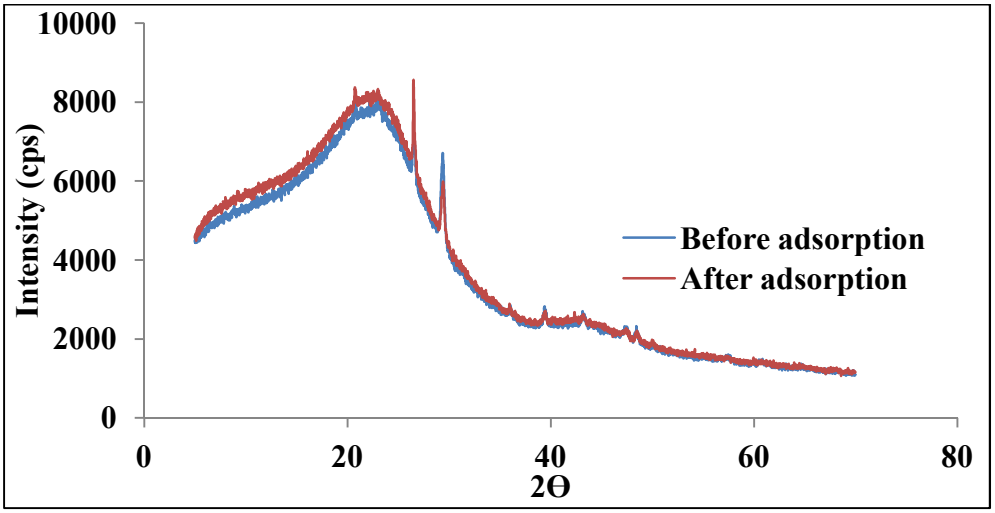

Fig. 6.2 XRD analysis of the biochar before and after Cr(VI) adsorption

XRD analysis is an effectual characterization technique that clarifies the amorphous or crystalline nature of biochar and Cr loaded biochar. The XRD pattern of biochar prior to and after adsorption is presented in Fig. 6.2. The figure describes appreciable amount of amorphous nature but two major peaks were detected in the samples at 2Θ of 26.5º and 29.5º that corresponds to quartz (SiO_2) and calcite in the biochar. However, after adsorption the results exhibited no considerable change in the peak positions but slight decrease in the peak intensity was noted at 2Θ of 29.5º that may be because of the adsorption of chromium ions onto its surface. No appreciable change in the XRD plots denotes physical adsorption process and chemical composition of the adsorbent were not altered after adsorption (Srivastava et al., 2017).

6.3.1.3 FTIR analysis

Fig. 6.3 (a) and (b) presents the FTIR characterizations for biochar before and after Cr(VI) adsorption. The FTIR study showed various peaks indicating intricate character of the biochar. Peaks in the wavenumber range from 3521.40 to 3268.77 cm^{-1} were showing the intermolecular hydrogen bonding of alcohols, phenols and carboxylic acids. At 3170.53 cm^{-1} a stretching vibration was assigned to N-H group of amines. C-H stretch of alkanes and alkenes was observed at 2943.17 cm^{-1} whereas H-C-H asymmetric stretch of alkane was indicated from the peak at 2855.59 cm^{-1}. At 1640.76 cm^{-1} the peak may be assigned to C=O stretch of aldehydes or ketones. Presence of nitro group (N=O stretch) may be supported by the stretching band at 1541.37 cm^{-1}. A small peak at 1428.04 cm^{-1} was noted that corresponds to O-H bend vibrations of carboxylic acids. Regions in between 1028.26 and 1004.69 cm^{-1} indicated the C-O stretch vibrations that may be of esters or ethers. However, after adsorption shift in the peak position of functional groups were observed and the difference in the peak positions is presented in Table 6.2. Shift in the peak positions after Cr(VI) uptake point towards the strong bonding and complexation of O-H, C-O, N-H, C-H, C=O functional groups with biochar surface. In addition, peaks at 1004.69 and 1640.76 cm^{-1} became unremarkable, that indicates changes in the C-O and C=O bonds after adsorption. From these results it is apparent that C-O, O-H, N-H, C-H, C=O and N=O groups are linked with Cr(VI) adsorption onto biochar. Functional groups C-O and C=O mainly account for adsorption on SS biochar.

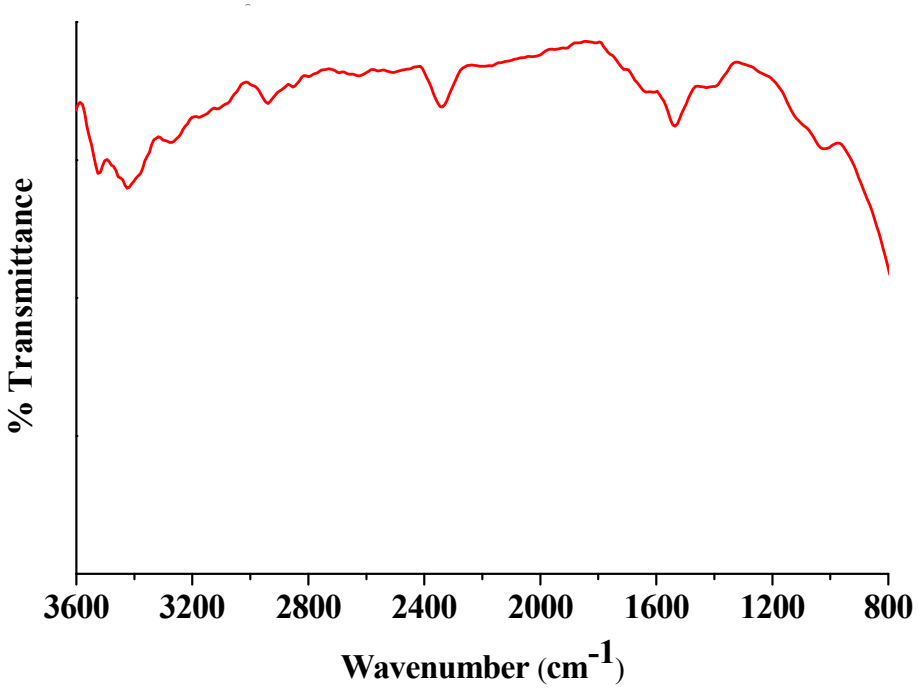

(a)

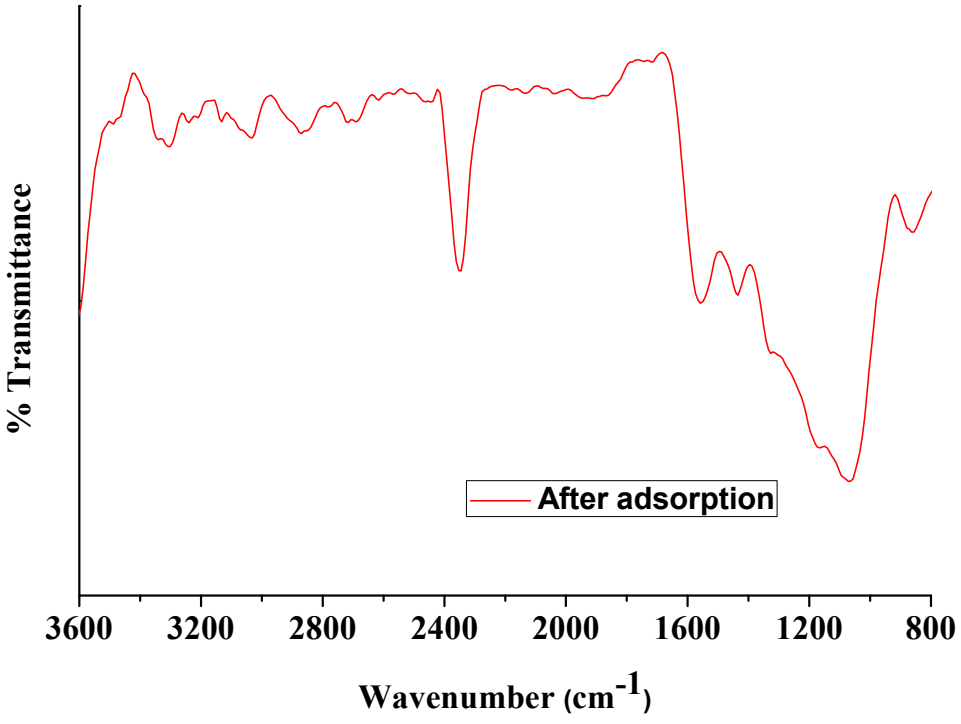

(b)

Fig. 6.3 FTIR spectra of biochar (a) before and (b) after adsorption of Cr(VI)

Table 6.2 FTIR analysis of biochar before and after adsorption of Cr(VI)

Peak position (cm^{-1})		Difference	Assignment
Before adsorption	**After adsorption**		
3521.40	3499.26	22.14	Hydrogen bonded O-H stretch
3423.16	3350.29	72.87	Hydrogen bonded O-H stretch
3268.77	3304.89	-36.12	Hydrogen bonded O-H stretch
3170.53	3144.57	25.96	N-H stretch of amines
2943.17	3031.07	-87.9	C-H stretch of alkanes and alkenes
2855.59	2874.30	-18.71	H-C-H asymmetric stretch alkanes
1640.76	-	-	C=O stretch of aldehydes or ketones
1541.37	1554.14	-12.77	N=O stretch of nitro group
1428.04	1438.52	-10.48	O-H bend vibrations of carboxylic acids
1028.26	1067.82	-39.56	C-O stretch of esters or ethers
1004.69	-	-	C-O stretch of esters or ethers

6.3.1.4 SEM-EDS analysis

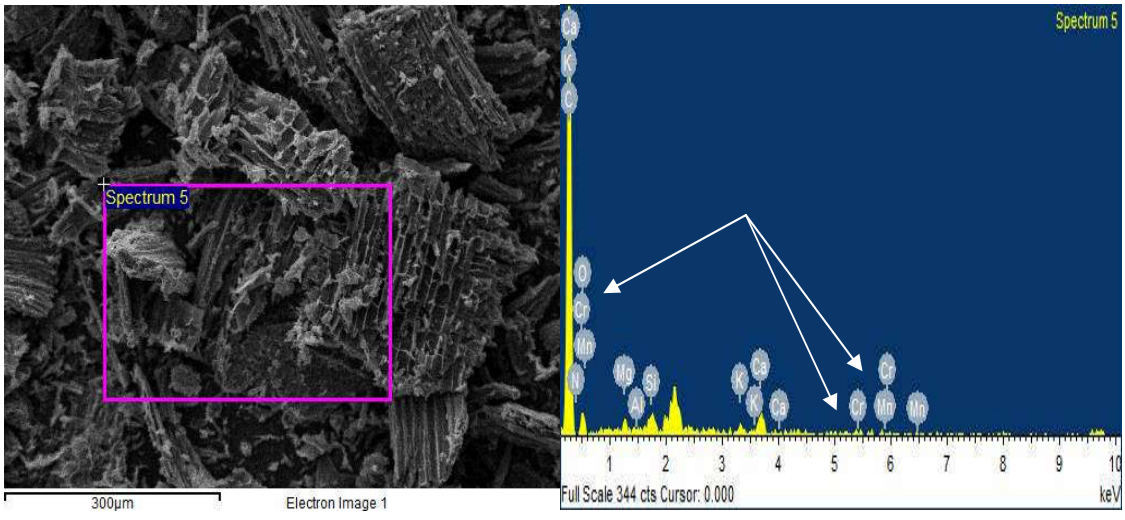

Fig. 6.4 SEM-EDS analysis of biochar after adsorption of Cr(VI)

From the SEM image it is clearly visible that adsorbent surface is smooth, porous and had ample number of pores in it before adsorption (discussed in section 5.3.5.1). After adsorption, the majority of the pores were blocked and broken showing saturation level for adsorption sites and also had corroded rough surface that might be caused by the uptake of Cr from solution as shown in Fig. 6.4. A fresh peak of Cr was detected in the EDS plot showing the reaction of Cr(VI) with biochar surface. This phenomenon indicates ion exchange or surface adsorption may be liable for Cr(VI) adsorption. Thus, EDS result affirmed the binding of Cr ions on biochar surface.

6.3.1.5 XPS analysis

XPS survey of biochar and Cr loaded biochar were performed in the wide and narrow scan to inspect the adsorption and reduction mechanism of Cr(VI) onto biochar as depicted in Fig. 6.5 and 6.6, respectively. Fig. 6.5 describes the wide scan analysis of the biochar before and after adsorption. A new peak was observed in between 570-590 eV on the biochar after adsorption that corresponds to the presence of Cr on the biochar. However, the oxidation state for Cr was investigated from the narrow scan results. In the narrow XPS spectrum for Cr (Fig. 6.6), two broad peaks were noted at around 586.33 and 576.71 eV for $Cr2p_{1/2}$ and $Cr2p_{3/2}$, respectively. However, these peaks can be further divided into 2 peaks each. Peak at 586.33 eV can be sub-divided into peaks at 588.32 and 586.24 eV that corresponds to $Cr2p_{1/2}$ of Cr(VI) and Cr(III), respectively. Similarly peak at 576.71 eV can be fitted into peaks at 578.65 and 576.59 eV that is assigned to $Cr2p_{3/2}$ of Cr(VI) and Cr(III), indicating existence of both the oxidation states for Cr on biochar surface. Similar result was observed by Mortazavian et al. (2019) in their research, i.e. Cr(VI) removal by modified activated carbon. Thus, the XPS result indicates the occurrence of adsorption in conjunction with reduction of Cr(VI).

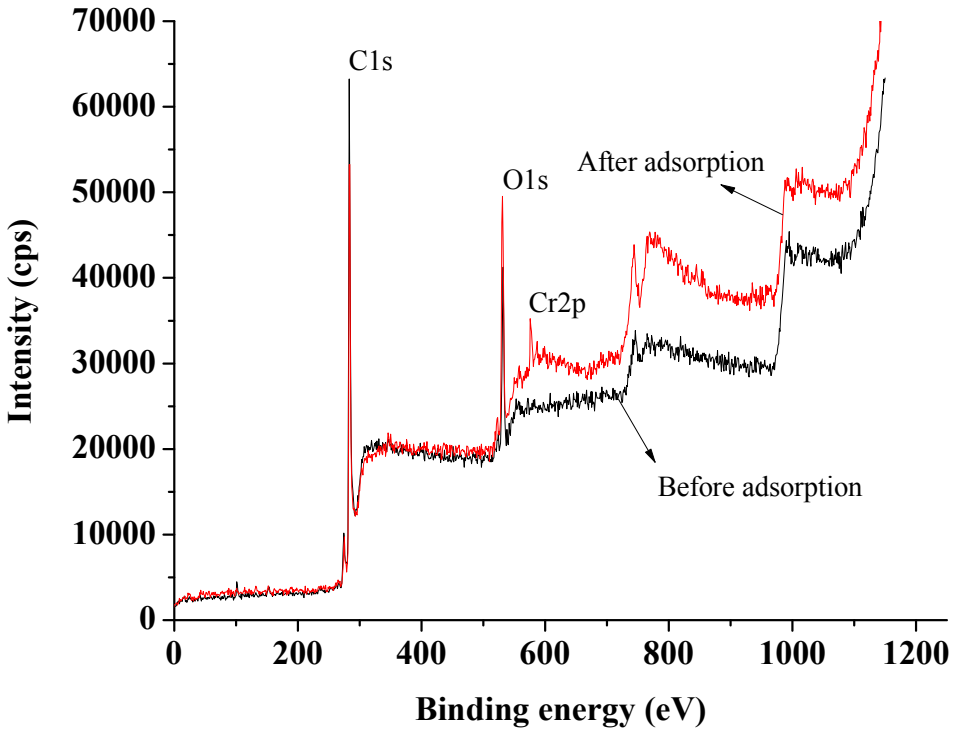

Fig. 6.5 Wide scan XPS analysis of the biochar after adsorption

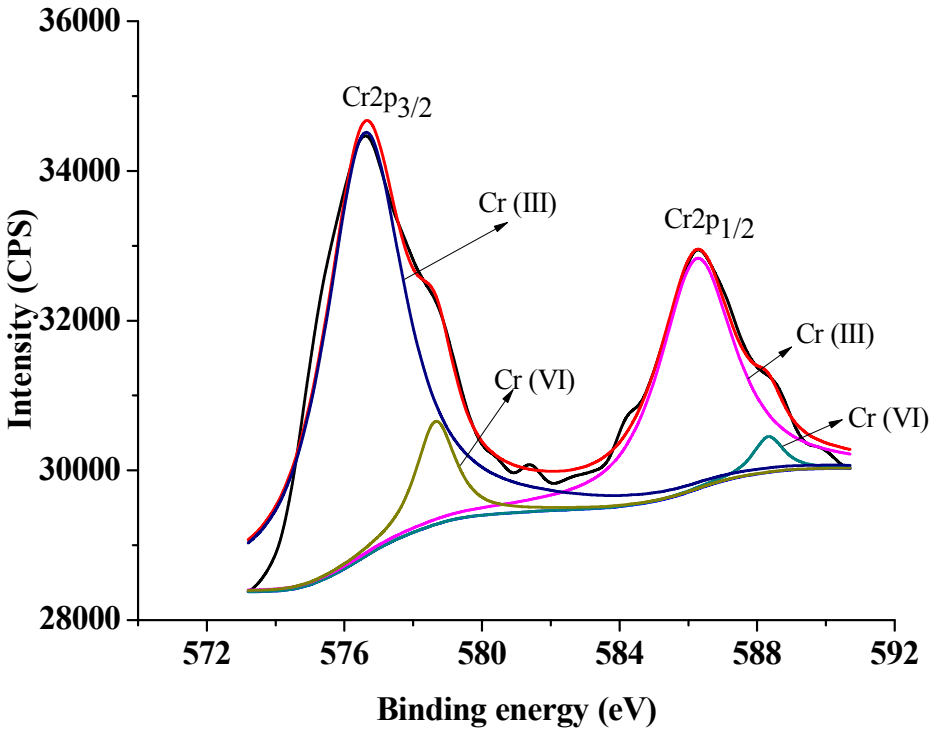

Fig. 6.6 Narrow scan XPS analysis for Cr after adsorption

6.3.2. Effect of process parameters

6.3.2.1 Effect of contact time and adsorbate concentration

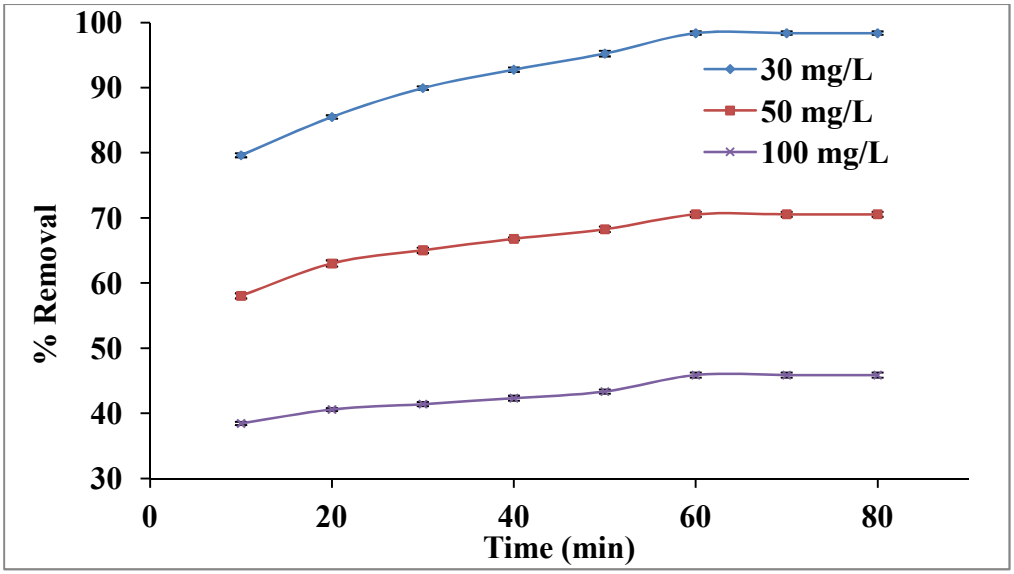

Fig. 6.7 Effect of initial concentration and contact time

Initial Cr(VI) concentration and contact time were investigated together for Cr(VI) adsorption onto biochar as depicted in Fig. 6.7. The results marked a significant decrease in the % removal with increase in metal ion concentration from 30 to 100 mg/L keeping other process variables (pH 2.0, adsorbent dose/Cr(VI) concentration 166.67 and temperature 30 °C) unchanged. According to Shekari et al. (2017), this decrease is because of the decline in adsorbentdose/Cr(VI) ion ratio, as active sites for the adsorbent was fixed and sites were covered up after attaining saturation leaving rest Cr(VI) ions unadsorbed. Simultaneously, outcome of contact time was also studied and the results illustrate increase in Cr(VI) uptake on biochar with as the contact time increased till equilibrium was achieved. The removal showed an increase from 79.63 to 98.37 % as the contacting time went on increasing from 10 to 60 min for 30 mg/L solution and beyond that % removal was constant. Thus, the equilibrium time for the

adsorption process was 60 min which is important to study the efficacy and feasibility of the adsorbent. The high adsorption efficiency can be endorsed to the reason that increased contact time provided enough time to chromate ions to find out binding sites for its adsorption (Nigam et al., 2019).

6.3.2.2 Effect of adsorbent dose/Cr(VI) concentration ratio

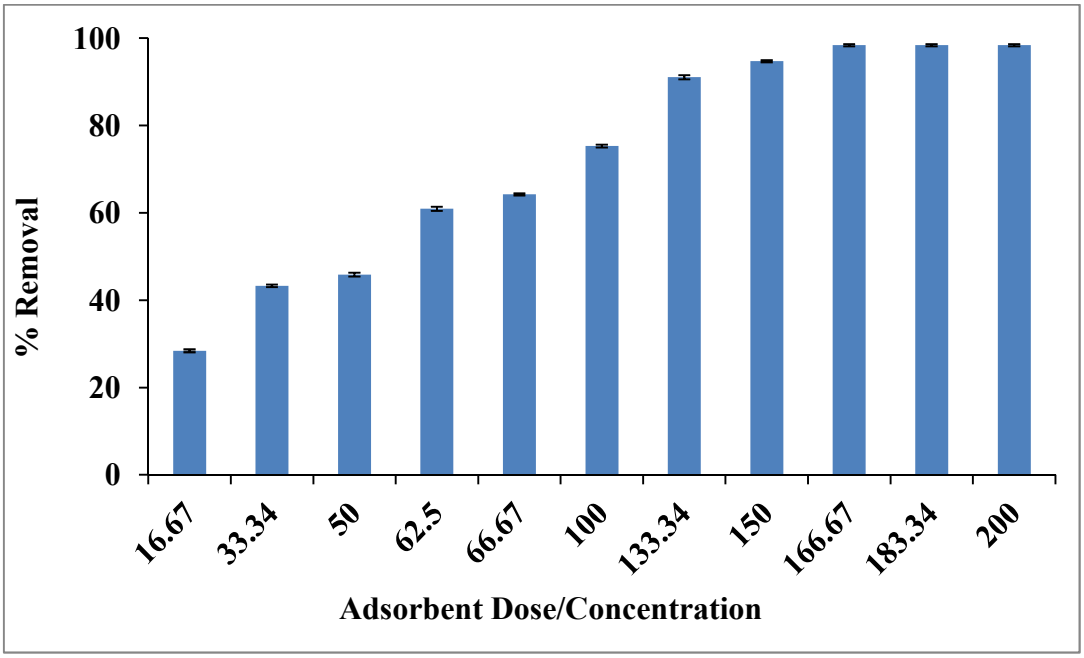

Fig. 6.8 Effect of adsorbent dose/Cr(VI) concentration ratio

The adsorbent dose/Cr(VI) concentration ratio was varied from 16.67 to 200 to find out its effect in removing Cr(VI) as portrayed in Fig. 6.8. As the ratio from 16.67 to 166.67, the % removal was enhanced from 28.41 to 98.37 % and after that the change in the result was insignificant. The possible reason for this may be, with increase in adsorbent amount, more active sites were present and the binding sites for the uptake of Cr(VI) ions. Similar phenomenon was also studied by Khosravi et al. (2014). However, further enhancement in the ratio didn't show much change in the removal that may be because

of binding of all the ions on the active sites of biochar building an equilibrium relation and keeping other sites vacant.

6.3.2.3 Effect of solution pH

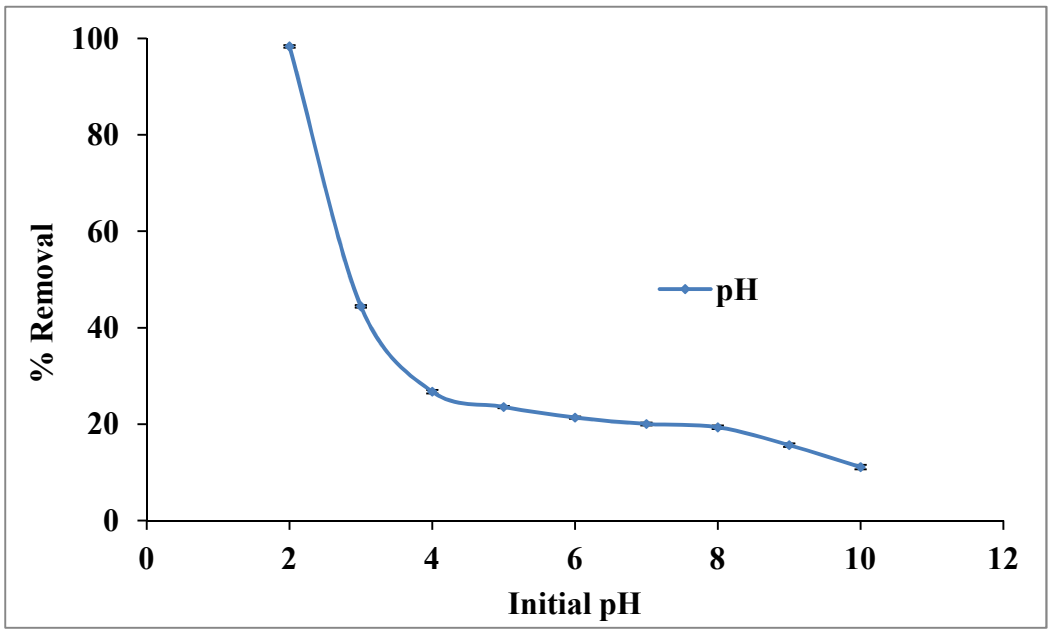

Fig. 6.9 Effect of solution pH

Initial pH of the solution is most essential and influencing variable for Cr(VI) adsorption. In the current study, variation in solution pH was done from 2 – 10 as presented in Fig. 6.9. It is apparent with the result that the Cr(VI) removal decreased sharply to 26.72 % from 98.37 % with increase in solution pH from 2 to 4. Thereafter the Cr(VI) removal trend was very less till pH 8 and finally beyond pH 8, the trend showed sudden decrease in Cr(VI) removal to 11.06 % at pH 10. The pH_{zpc} of the adsorbent was found to be 8.4 which means beyond this pH removal efficiency is very low and it is in agreement with the result. The reason for this may be that at high acidic pH, $HCrO_4^-$ is the leading form of Cr which is getting adsorbed on the adsorbent surface

because of its lower adsorption free energy change whereas at higher pH this $HCrO_4^-$ gets converted to CrO_4^{2-} and $Cr_2O_7^{2-}$ (Kapur and Mondal, 2013). But at higher pH there is competition between OH^- and CrO_4^{2-} , $Cr_2O_7^{2-}$ species for the same active site, thus there is lower efficiency in removal at high basic pH. In addition, surface of the adsorbent has positive charge at higher acidic pH and it binds $HCrO_4^-$ (anionic species) by electrostatic attraction (Nigam et al., 2019).

6.3.2.4 Effect of temperature

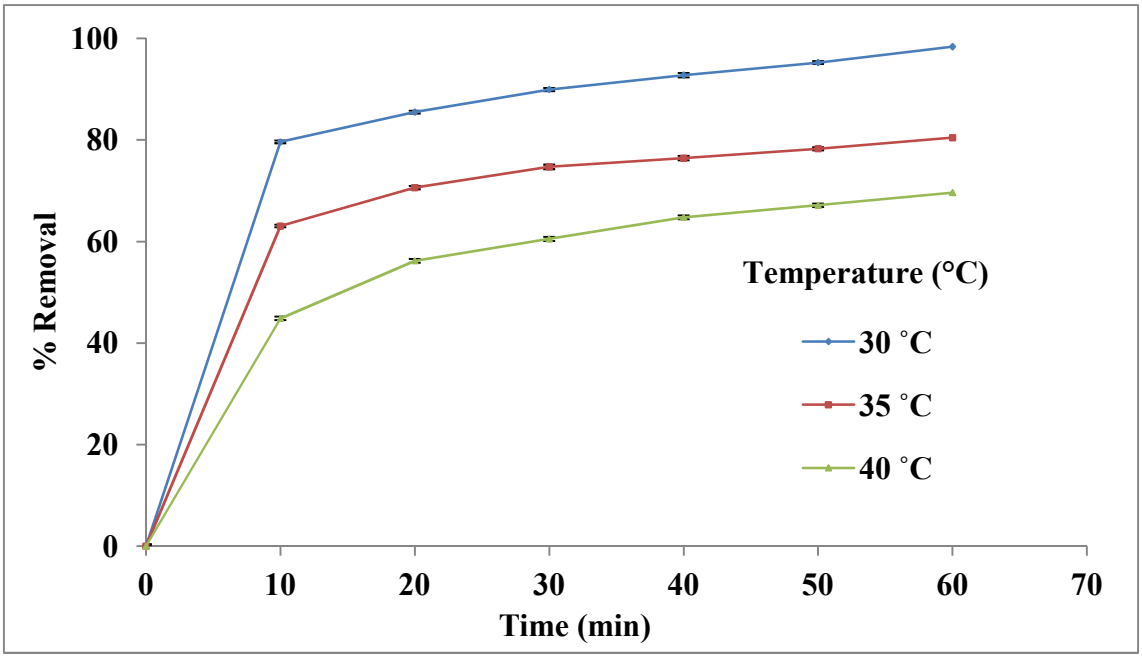

Fig. 6.10 Effect of temperature

Temperature had prominent effect on Cr(VI) removal as portrayed in Fig. 6.10. For the effect of temperature, temperature variation was done from 30 to 40 °C at fixed Cr(VI) concentration of 30 mg/L, pH 2 and adsorbent dose/Cr(VI) concentration 166.67 till equilibrium time. The results revealed maximum adsorption at 30 °C followed by

decrease in the adsorption of Cr(VI) as the temperature progressed from 30 to 40 °C. Variation of temperature in the study is helpful in predicting the nature of adsorption. The present study confirmed the process to be exothermic as adsorption of metal ions decreased with increased system temperature. The temperature increment accelerated the metal ions mobility resulting in desorption of metal ions from active sites and thus also signifies no chemical bonding between the adsorbate and adsorbent (Owalude and Tella, 2016)

6.3.3 BBD and statistical analysis

The study of design and statistics for the adsorption process was done using State-Ease Design Expert software. The BBD provided total 17 experimental runs (including 5 centre runs) with 3 independent variables (pH, temperature and dose/Cr(VI) concentration ratio) at 3 levels (-1, 0, 1) and the responses were recorded derived from the quadratic model as suggested by sequential model sum of squares. The results (actual and predicted) from the experimental runs are provided in Table 6.3. To figure out a standard relation between independent (process variables) and dependent variable (responses), regression analysis was performed. The actual (experimental) and predicted (from software) results for Cr(VI) removal showed very close relationship as R^2 value was very near to 1 as shown in Fig. 6.11. The result proposed a strong relationship between the predicted and actual responses and so % Cr(VI) removal can be predicted from the developed model. The final empirical equation in terms of coded independent variables (A = pH, B = Temperature, C = Dose/Cr(VI) concentration) is shown below.

$$\textbf{\% Cr(VI) Removal} = 65.51 - 18.42\,A - 6.23\,B + 5.35\,C + 5.41\,AB - 1.67\,AC - 0.75BC - 6.89\,A^2 + 0.53\,B^2 - 0.74\,C^2 \quad (6.4)$$

The response was expressed as % Cr(VI) removal as depicted in equation 4. From the linear terms, only dose/Cr(VI) concentration has positive relationship with the removal favouring the optimization process whereas pH and temperature has inverse response.

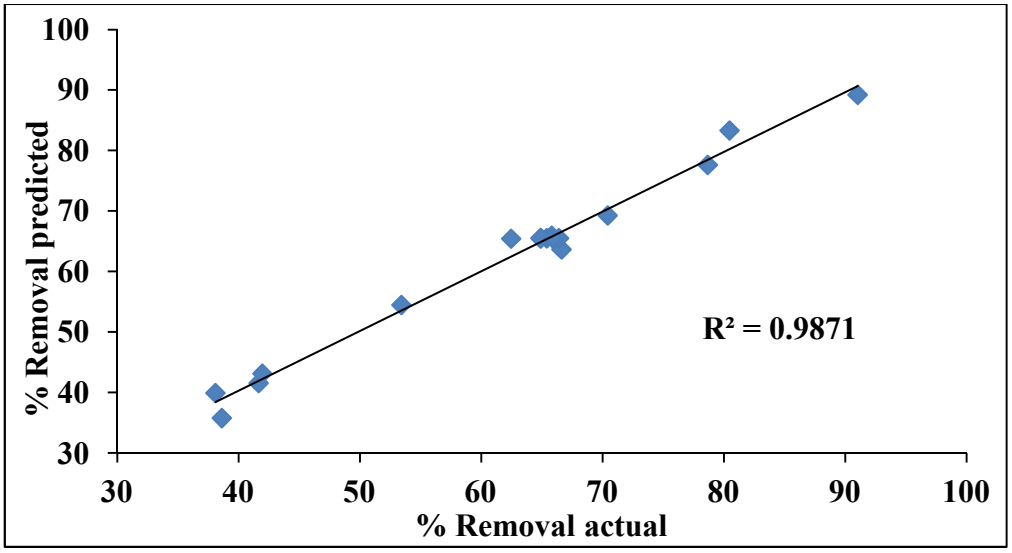

Fig. 6.11 Actual vs predicted values of the model for Cr(VI) removal

ANOVA was performed to ascertain the reliability of the quadratic model in % Cr(VI) removal as illustrated in Table 6.4. The agreement of the developed model is dependent on the F-value (Fischer test value) and p-value (probability value). Lower p-value (< 0.05) designates the significance of the model whereas high F-value illustrates the superior dependability of the model (Arvindekar and Laddha, 2016). In the present work, F-value for the model was 59.53 and prob > F (p value) was less than 0.0001 showing model is both satisfactory and significant. Among the linear terms, pH was most significant parameter in the adsorption process having highest F value of 405.10 whereas temperature and dose/Cr(VI) concentration showed moderate effect. However, the significant terms for the study were A, B, C, AB and A^2. Based on the sum of square values, the linear terms along with AB, A^2 have significant effect on the removal process whereas AC, BC, B^2 and C^2 has little or insignificant effect. The standard

deviation (SD) and mean responses for the process was 2.59 and 62.17, respectively. A very small SD is acceptable as it implies great model fitting for the optimization process.

Table 6.3 Box-Behnken experimental design matrix and results

Run	pH	Temperature (°C)	Dose/ Concentration	Actual % removal	Predicted % removal
1	2.50	30	166.67	78.67	77.63
2	2.50	35	133.33	65.41	65.51
3	2.00	35	100.00	70.43	69.27
4	3.00	30	133.33	41.67	41.55
5	2.00	40	133.33	65.81	65.93
6	2.50	35	133.33	64.91	65.51
7	2.50	30	100.00	62.47	65.43
8	2.50	40	166.67	66.63	63.66
9	2.50	35	133.33	66.41	65.51
10	3.00	40	133.33	38.11	39.92
11	2.50	40	100.00	53.43	54.47
12	3.00	35	100.00	38.63	35.78
13	2.50	35	133.33	64.91	65.51
14	2.50	35	133.33	65.91	65.51
15	3.00	35	166.67	41.97	43.13
16	2.00	30	133.33	91.03	89.22
17	2.00	35	166.67	80.47	83.32

The relative SD for the process is measured by co-efficient of variation (CV) and for the present study it was 4.16 %. A value less than 10 % is desirable for better reproduction of results and greater reliability (Mohammed et al., 2017). The R^2, Adj-R^2 and Pred-R^2 values for the process were 0.9871, 0.9705 and 0.8004, respectively showing good

fitting of the empirical data with the model. A good conformity was seen for Adj-R^2 with Pred-R^2. The R^2 value of 0.9871 signifies 98.71 % of the variation in Cr(VI) adsorption was predictable by the model and rest was estimated by deviation in residual.

Table 6.4 ANOVA analysis for Cr(VI) removal

Source	Sum of Squares	df	Mean Square	F Value	p-value Prob > F	
Model	3589.77	9	398.86	59.53	< 0.0001	Signi-ficant
A-pH	2714.37	1	2714.37	405.10	< 0.0001	
B-Temperature	310.75	1	310.75	46.38	0.0003	
C-Dose/ Concentration	228.77	1	228.77	34.14	0.0006	
AB	117.29	1	117.29	17.50	0.0041	
AC	11.22	1	11.22	1.67	0.2367	
BC	2.25	1	2.25	0.34	0.5804	
A^2	199.88	1	199.88	29.83	0.0009	
B^2	1.21	1	1.21	0.18	0.6842	
C^2	2.34	1	2.34	0.35	0.5734	
Residual	46.90	7	6.70			
Lack of Fit	45.20	3	15.07	35.45	0.0024	
Pure Error	1.70	4	0.42			
Cor Total	3636.67	16				
Std. Dev.	2.59		R-Squared		0.9871	
Mean	62.17		Adj R-Squared		0.9705	
C.V. %	4.16		Pred R-Squared		0.8004	
PRESS	725.91		Adeq Precision		26.92	

The adequate precision i.e. noise to signal ratio for the developed model was 26.918. It measures the series of expected response along with the errors associated with it. Thus,

the statistical summary suggests that the statistical model is valid and can perfectly drive the design space.

6.3.4 Optimization and three-dimensional plots

Numerical optimization technique was followed for the maximization of Cr(VI) removal considering three process variables (pH, temperature and dose/Cr(VI) concentration) and keeping them in the same experimental condition range. In addition, 3-D surface plots generated were used to discover the outcome of process variables on responses and their interactive effect. The RSM 3-D plots for Cr(VI) removal is represented in Fig. 6.12 varying two variables and maintaining the third factor stable.

6.3.4.1 Optimization of temperature and initial pH

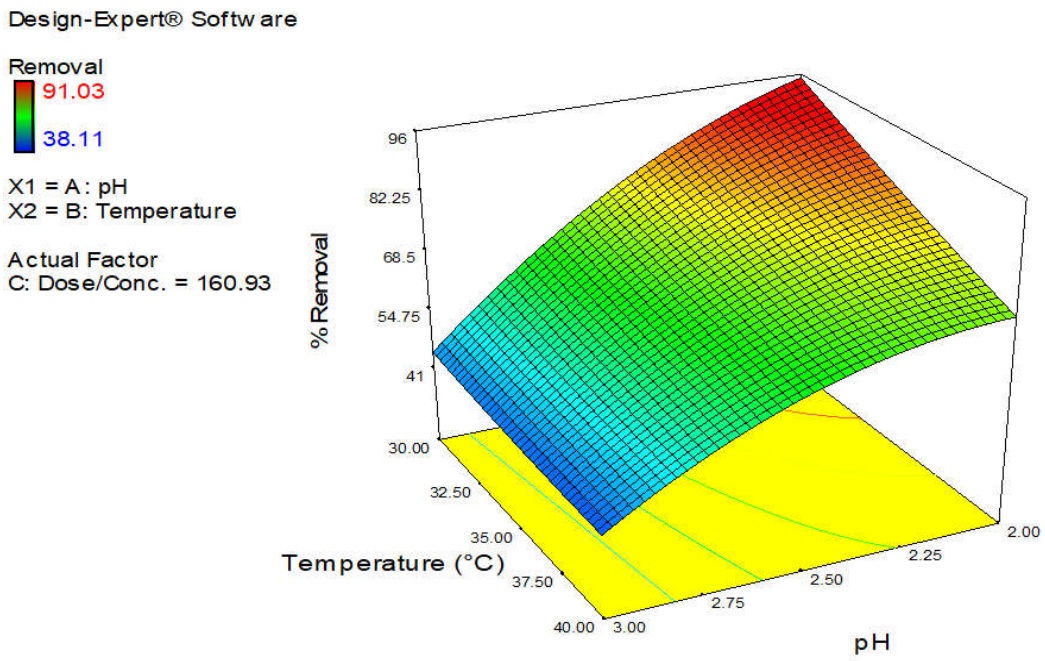

Fig. 6.12 3-D surface response for % removal of Cr(VI) showing interaction effects of temperature and pH

The 3-D surface plots showing the interaction effect of temperature and initial pH of adsorbate in Cr(VI) removal is shown in Fig. 6.12 keeping dose/Cr(VI) concentration fixed at 160.93. It is inferred from the figure that both the variables have immense effect on the adsorption process as with increase in the temperature and pH there is decrease in the removal of Cr(VI). The high amount of removal at lower pH is mainly owing to the more positivity of the surface leading to adsorption of Cr(VI) in the form of negatively charged chromate ions i.e. $HCrO_4^-$ (Dubey et al., 2016). Also, increase in the temperature may lead to desorption of some of the metal ions or increase their mobility showing lesser adsorption at active sites and thus decreasing the removal of Cr(VI) at higher temperature (Owalude and Tella, 2016).

6.3.4.2 Optimization of initial pH and adsorbent dose/Cr(VI) concentration

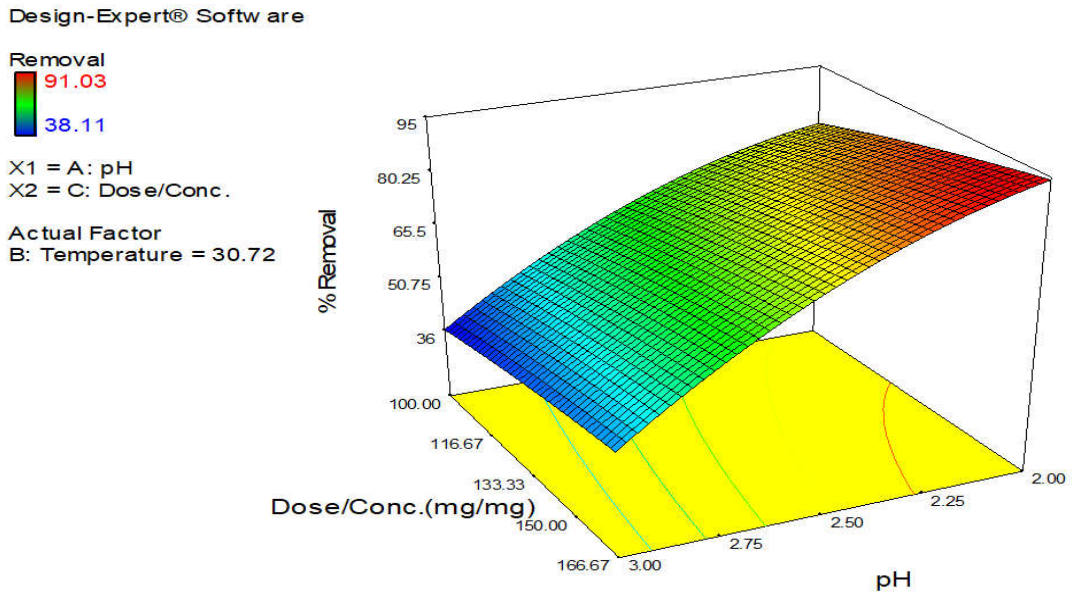

Fig. 6.13 3-D surface response for % removal of Cr(VI) showing interaction effects of dose/Cr(VI) concentration and pH

The interactive effect of dose/Cr(VI) concentration and initial pH of adsorbate on Cr(VI) removal is illustrated in Fig. 6.13 where temperature was fixed at 30.72 °C. Increasing the dose/Cr(VI) concentration ratio marked high increment in the Cr(VI) removal however increasing pH showed decreasing trend. This tendency is likely since increase in the adsorbent dose creates more amounts of active sites and thus more Cr(VI) ions are attached to their surfaces showing more removal.

6.3.4.3 Optimization of adsorbent dose/Cr(VI) concentration and temperature

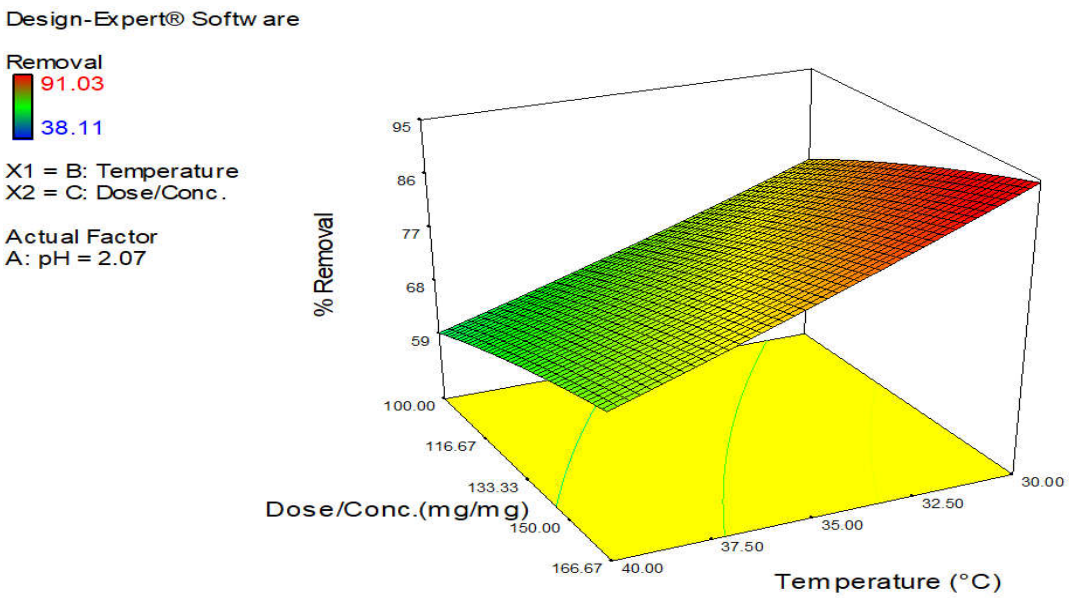

Fig. 6.14 3-D surface response for % removal of Cr(VI) showing interaction effects of dose/Cr(VI) concentration and temperature

Regarding the interactive effect of dose/Cr(VI) concentration and temperature on Cr(VI) removal at constant pH of 2.07, the 3-D plot is shown in Fig. 6.14. The figure describes the inverse relationship between dose/Cr(VI) concentration ratio and temperature. Temperature increase might have enhanced the mobility of the ions and in

addition more active sites with increase in dose/Cr(VI) concentration ratio provided more binding sites for metal ions on adsorbent surface.

6.3.4.4 Validation of optimized result

To validate the optimized condition achieved after numerical modelling, the confirmatory experiments were performed. The optimized conditions for predicted maximum Cr(VI) were pH 2.07, temperature 30.72 °C and dose/Cr(VI) concentration 160.93 with desirability of 1. To affirm the optimized result, the process was repeated in triplicate at optimized conditions and the results were comparable as concised in Table 6.5. The maximum removal for Cr(VI) was 90.89 % at pH 2.07, temperature 30.72 °C and dose/Cr(VI) concentration 161. The divergence between the investigated and predicted results was negligible signifying the sufficiency of the model.

Table 6.5 Cr(VI) removal predicted and experimental values at optimized condition

Parameters			% Removal	
pH	Temperature (°C)	Adsorbent dose/Cr(VI) concentration		
2.07	30.72	160.93	91.72	Predicted
2.07	30.72	161	90.89	Experimental

6.3.5 Adsorption kinetics study

Kinetic study for the adsorption process is very essential as it illustrates the adsorbate adsorption rate at solid-liquid interface depending on different reactions at the surface. The adsorption mechanism is greatly reliant on physico-chemical characteristics of biochar including mass transfer phenomena as it is a complex process. In this research, the adsorption data collected from effect of temperatures with time were used for the

kinetic studies. The rate kinetics for Cr(VI) uptake was examined by both first and second order model. The standard equation for both the models is described below.

The first order kinetics is given by:

$$\ln\ (q_e - q_t) = \ln q_e - k_1 t \qquad (6.5)$$

In which, qt and qe (mg/g) denotes the adsorption uptake of Cr(VI) at any time t (min) and at equilibrium and k_1 denotes the first order rate constant (min^{-1}).

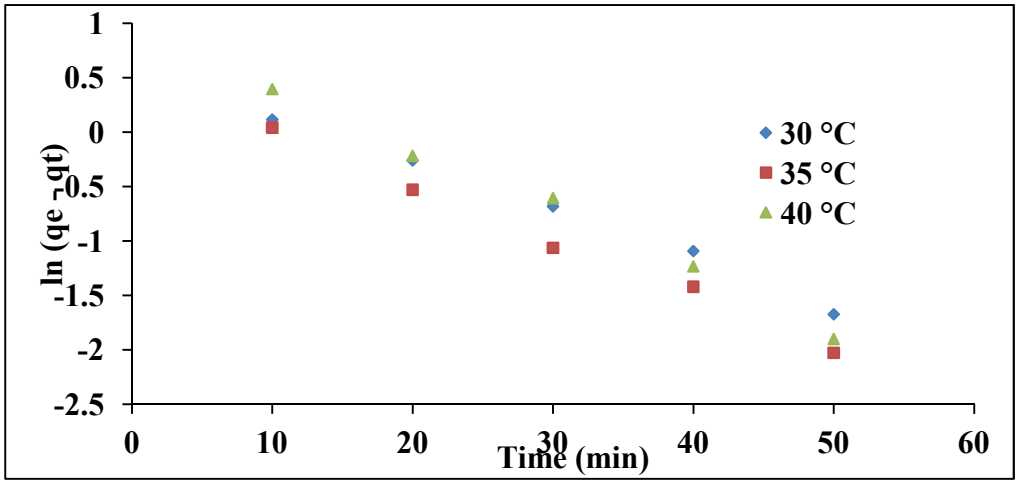

Fig. 6.15 1st order kinetic model for Cr(VI) adsorption using biochar

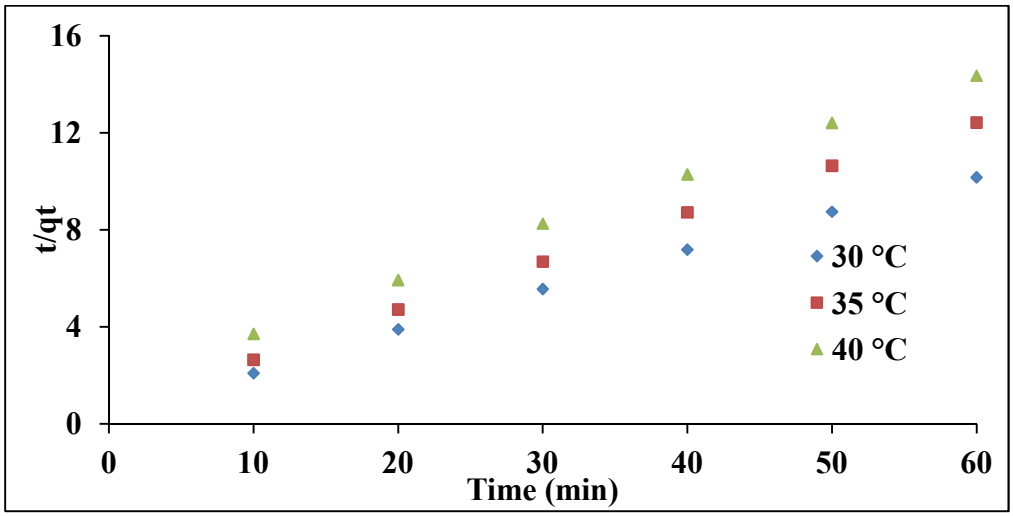

Fig. 6.16 2nd order kinetic model for Cr(VI) adsorption using biochar

Similarly, second order rate equation is given by:

$$\frac{t}{q_t} = \frac{1}{k_2\, q_e^2} + \frac{t}{q_e} \qquad \textbf{(6.6)}$$

Where, k_2 (g/mg.min) represents rate constant for second order. Graphical representation for both the kinetic models is displayed in Fig. 6.15 and 6.16, respectively and the kinetic parameters are represented in Table 6.6. As per regression co-efficient value (R^2), experimental results fitted well with second order equation relative to first-order kinetics and thus the adsorption process is following the second order kinetics.

Table 6.6 Kinetics constants for Cr(VI) adsorption onto biochar

Temperature (°C)	First-order kinetics			Second-order kinetics		
	K_1 (min^{-1})	qe (mg/g)	R^2	K_2 (g/mg.min)	qe (mg/g)	R^2
30	0.044	1.831	0.993	0.0419	6.211	0.998
35	0.050	1.665	0.994	0.050	5.102	0.999
40	0.056	2.637	0.993	0.0268	4.695	0.999

6.3.6 Thermodynamic study

Thermodynamic study was done to learn the nature of adsorption process as well as to find out the thermodynamic properties (ΔG°, ΔH° and ΔSº). Following equations were used for the calculation of different parameters:

$$\Delta G^o = -RT \ln k_c \qquad \textbf{(6.7)}$$

$$K_c = \frac{C_{Ae}}{C_e} \qquad \textbf{(6.8)}$$

$$\ln K_c = \frac{\Delta S^o}{R} - \frac{\Delta H^o}{RT} \qquad \textbf{(6.9)}$$

Where, C_{Ae} and C_e are the concentration for Cr(VI) onto biochar and in supernatant at equilibrium, K_c is the dimensionless equilibrium constant. Thermodynamic parameters were computed using the slope and intercept of ln K_c vs. 1/T plot and the results are presented in Table 6.7. –ve values for ΔG^o at all three temperatures suggest that the process feasibility as well as its spontaneous nature. The –ve value for ΔH^o signifies the process to be exothermic in nature and –ve ΔS^o refers to the lowering in the randomness at the biochar-Cr(VI) interface all through the adsorption.

Table 6.7 Thermodynamic Parameters for Cr(VI) adsorption onto biochar

Thermodynamic parameters	Temperatures (°C)		
	30	35	40
ΔG (kJ/mol)	-10.32	-3.63	-2.16
ΔH (kJ/mol)	-258.67		
ΔS (kJ/mol.K)	-0.82		

The iso-steric heat of adsorption (ΔH_r) for the process was obtained using the below equation:

$$\Delta \boldsymbol{H_r} = \left(\frac{\boldsymbol{R} \ln \frac{\boldsymbol{C_y}}{\boldsymbol{C_x}}}{\left(\frac{\boldsymbol{1}}{\boldsymbol{T_y}} - \frac{\boldsymbol{1}}{\boldsymbol{T_x}} \right)} \right) \quad \textbf{(6.10)}$$

Where, C_x, C_y denotes adsorbate concentration at equilibrium for the temperatures T_x, T_y and R is universal gas constant. The calculated result for ΔH_r is -230.45 kJ/mol suggesting the process to be of exothermic nature.

6.3.7 Adsorption isotherms

The adsorption phenomena can be better understood after studying the different isotherms. The isotherms relate the ions concentration in the liquid as well as quantity

of ions up taken per unit mass of biochar at invariable temperature in equilibrium. Here, 4 different isotherms (Langmuir, Freundlich, Temkin and Dubinin-Radushkevich (D-R)) were employed. The isotherm constants are presented in Table 6.8.

6.3.7.1 Langmuir isotherm

It is the most common type adsorption isotherm studied by many researchers that basically assumes adsorption occurs in monolayer with all active sites having equivalent attraction for the adsorbate to adsorb (Langmuir et al., 1918). In addition, adsorption at one particular active spot doesn't affect the uptake of adsorbate to another site. The linearized Langmuir equation is shown below:

$$\frac{C_e}{q_e} = \frac{1}{Q_0 b} + \frac{C_e}{Q_o} \quad \textbf{(6.11)}$$

Where, C_e (mg/L) implies equilibrium concentration, q_e (mg/g) is the quantity adsorbed per unit weight of adsorbent, Q_0 (mg/g) denotes maximum adsorption capacity and b (L/mg) represents isotherm constant, respectively. The graph of C_e/q_e vs C_e gives equation of a straight line where slope was used to calculate Q_0 and intercept for the calculation of b. Declining of Q_0 and b values with rise in temperature is indicative that the process is exothermic (AL-Othman et al., 2012).

A dimension less parameter R_L (Separation factor) was considered to ensure the favourability of the adsorption process based on the isotherm constant b from Langmuir model (Tang et al., 2013). The expression for R_L is presented below:

$$R_L = \frac{1}{1 + bC_O} \quad \textbf{(6.12)}$$

Where, C_0 and b denotes the initial Cr(VI) concentration (mg/L) and isotherm constant (L/mg), respectively.

The isotherm results are presented in Table 6.8. All R^2 values are very near to 1and R_L values in between 0 – 1 indicates favourable model in adsorbing Cr(VI) using biochar.

6.3.7.2 Freundlich isotherm

This isotherm model explains the multilayer adsorption (adsorption site has affinity for more than 1 adsorbate ion) of the chromate ions on the heterogeneous adsorbent surface (Freundlich et al., 1906). The linearized equation is expressed by:

$$\ln q_e = \ln K_f + \frac{1}{n} \ln C_e \quad (6.13)$$

Where, 1/n relates to intensity of the adsorbent and Freundlich equilibrium constants K_f to adsorption capacity. The values were obtained using the slope and intercept from the plot of ln q_e vs. ln C_e. The results from the isotherm model are shown in Table 6.8. The results for 1/n in the range from 0 – 1 specify favourable conditions for adsorption. However, poorer R^2 value in between 0.807 - 0.926 remarks unsuitability of this isotherm for Cr(VI) uptake on SS biochar.

6.3.7.3 Temkin isotherm

It relates the contact of Cr(VI) ions with the heterogeneous surface of the biochar. Its assumption says that with increase in the surface coverage, heat of adsorption decreases linearly and there is uniformity in the distribution of binding energies (Temkin and Pyzhev, 1940). The lineralized equation is presented below:

$$q_e = \frac{RT}{h} \ln K_T + \frac{RT}{h} \ln C_e \quad (6.14)$$

In which, K_T (L/g) corresponds to Temkin constant, h (kJ/mol) is interrelated with heat of adsorption, R is universal gas constant (8.314 J/mol.K) and T (K) is temperature. From the linear plot of q_e vs. ln C_e, the constants were derived and are presented in Table 6.8. The values for h < 8 kJ/mol signify weaker interactions between biochar and ions i.e. some of the Cr ions are released to the solution (Wahab et al., 2017). But the R^2 values for the model were in the range of 0.760-0.902 and thus Temkin model is not as good as other two models as described above.

6.3.7.4 Dubinin-Radushkevich (D-R) isotherm

It relates the adsorption of Cr(VI) ions on to the porous structure of the adsorbent. The linearized equation is presented below:

$$\ln q_e = \ln q_{DR} - K_{DR}\,\varepsilon^2 \qquad (6.15)$$

In which, q_{DR} (mg/g) and K_{DR} (mol^2/kJ^2) denotes the maximum adsorption capacity and activity co-efficient. ε represents the Polanyi potential derived from the equation mentioned beneath:

$$\varepsilon = RT \ln\left(1 + \frac{1}{C_e}\right) \qquad (6.16)$$

This isotherm mainly gives the idea if the process is of physical or chemical nature (Choudhary and Paul, 2018) and thus mean adsorption energy (E) was obtained from the below equation:

$$E = \frac{1}{\sqrt{2K_{DR}}} \qquad (6.17)$$

E as calculated using the constants derived from the graph of ln qe vs. ε^2 was less than 8 kJ/mol signifying physical adsorption for Cr(VI) onto biochar. However, very low regression co-efficient (R^2) suggests (Table 6.8) that D-R isotherm do not have good concurrence with the experimental data.

Table 6.8 Langmuir, Freundlich, Temkin and D-R isotherm constants for Cr(VI) adsorption onto biochar

Isotherms	Temperatures (°C)		
	30	35	40
Langmuir constants			
Q_0 (mg g^{-1})	9.62	9.26	7.69
b (L mg^{-1})	0.56	0.15	0.11
R^2	0.987	0.982	0.985
R_L	0.06	0.18	0.23
Freundlich constants			
K_F (mg/g)/(mg/L)^n	6.184	3.046	2.323
1/n	0.10	0.25	0.26
R^2	0.807	0.912	0.926
Temkin constants			
K_T (L/g)	4382.61	3.07	1.98
h (kJ/mol)	3.40	1.58	1.84
R^2	0.760	0.881	0.902
D-R constants			
q_{DR} (mg/g)	8.61	10.67	6.40
E (kJ/mol)	3.23	0.33	0.29
R^2	0.641	0.943	0.778

6.3.8 Mass transfer studies

Adsorption of a metal ion onto any adsorbent is a step by step process. Initially it starts with film diffusion i.e. metal ions from the solution bulk moves towards adsorbent surface. The metal ions are then accepted by the adsorbent surface. Thereafter particle diffusion occurs during which the adsorbate molecules enter into the interstitial spaces known as interparticle diffusion and then gets attached on the pores available on the

adsorbent surface. To figure out the rate determining step, Weber-Morris and Boyd models were employed as shown in Fig. 9 (a) and (b), respectively.

6.3.8.1 Weber-Morris model

During the batch mode process, it is assumed that mass may be transported through diffusion. Thus to investigate the mass transfer phenomena, a graphical method was investigated by Weber and Morris (1964) to find out if intraparticle diffusion is the rate determination step for the adsorption process. The linear form for the model is:

$$q_t = K_{id}\, t^{0.5} + C \qquad (6.18)$$

Where, qt (mg/g) is the amount of metal ion adsorbed on biochar, K_{id} (mg/g-$min^{0.5}$) is the model constant and C is also another constant that relates to thickness of boundary layer.

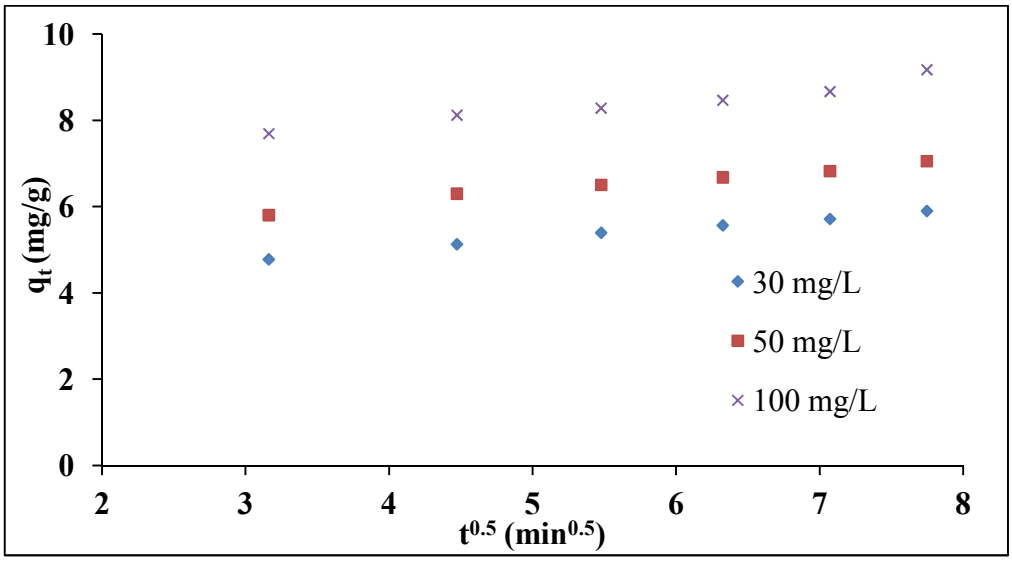

Fig. 6.17 Weber-Morris plot for adsorption of Cr(VI) using biochar

According to the assumptions, if the linear graph of q_t vs K_{id} pass through the origin i.e C=0, in that case the given model is considered the rate determination step. However, in

the present study C ≠ 0 and hence beside intraparticle diffusion, film diffusion may also be involved in the process. The values for K_{id} were 0.24, 0.256 and 0.287 mg/g.min$^{0.5}$ for 30, 50 and 100 mg/L Cr(VI) concentrations, respectively. Increase in K_{id} value with the increasing Cr(VI) concentration suggests faster diffusion and higher concentration driving force. The Weber-Morris plot is shown in Fig. 6.17.

6.3.8.2 Boyd model

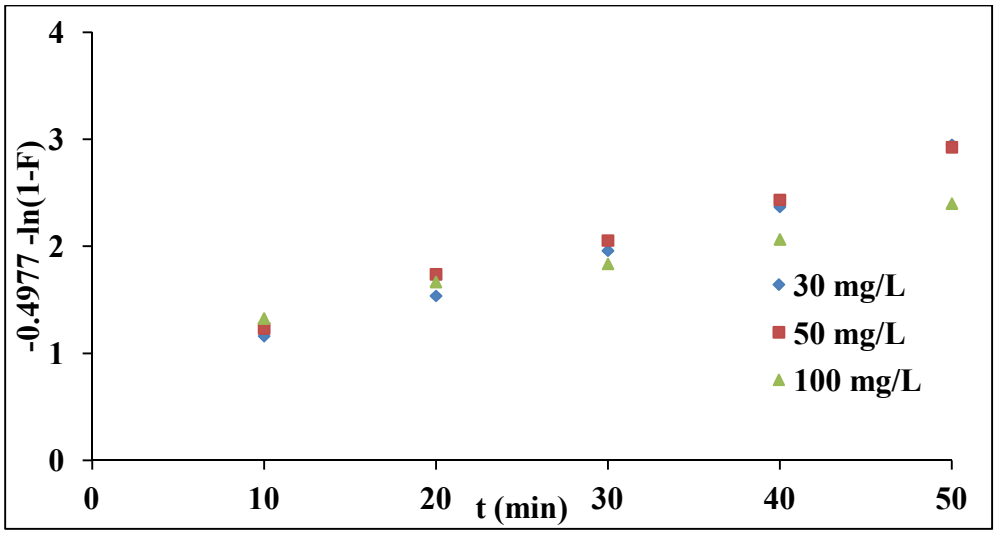

Fig. 6.18 Boyd plot for adsorption of Cr(VI) using biochar

Since the process is not only controlled by inter particle diffusion, thus Boyd model was applied for the determination film diffusion data. The model can be presented as:

$$F = 1 - \frac{6}{\pi^2} e^{-Bt} \qquad (6.19)$$

Where, $F = q_t/q_e$ and it describes the adsorbate adsorbed at time t and Bt is a function related to F. Equation (19) can be rephrased to:

$$Bt = [-0.4977 - \ln (1- F)] \qquad (6.20)$$

A linear graph of Bt vs. [-0.4977 – ln (1- F)] showed that the lines are not passing through origin and has intercept in all three cases as shown in Fig. 6.17. Thus the process is governed by the film diffusion. The effective diffusivity D_i (cm^2/s) was obtained using equation shown below.

$$\boldsymbol{B = \frac{\pi^2 D_i}{r^2}} \quad \textbf{(6.21)}$$

Where, r is the geometric mean radius of the particle. D_i values for the adsorption process were 4.93×10^{-7}, 4.48×10^{-7} and 2.81×10^{-7} cm^2/s for 30, 50 and 100 mg/L Cr(VI) concentrations, respectively. The Weber-Morris constant and effective diffusivities at different concentrations is presented in Table 6.9.

Table 6.9 Weber-Morris constants and effective diffusivity for Cr(VI) adsorption

Conc. (mg/L)	**K_{id} (mg g^{-1} $min^{0.5}$)**	**Constant: C (mg g^{-1})**	**R^2**	**B (s^{-1})**	**Geometric mean particle size (mm)**	**Effective diffusivity D_i (cm^2 s^{-1})**	**R^2**
30	0.240	4.043	0.996	0.044	0.2104	4.93×10^{-7}	0.993
50	0.256	5.066	0.982	0.04	0.2104	4.48×10^{-7}	0.994
100	0.287	6.758	0.943	0.025	0.2104	2.81×10^{-7}	0.987

6.3.9 Adsorption mechanism

Based on the findings, a reaction mechanism has been anticipated for Cr(VI) adsorption on SS biochar as displayed in Fig. 6.19. Cr(VI) adsorption on biochar surface occurs in multiple ways like porous or physical adsorption, complexation with functional groups, electrostatic attraction and also reduction. The physical adsorption on the biochar surface was confirmed by the appearance of Cr peak on the EDS analysis. In addition to it, FTIR spectra of biochar after adsorption showed functional groups like C-O, C=O,

C-H etc played a vital role in Cr(VI) adsorption and that may be because of the formation of complex bonds of Cr ions with surface functional groups. Initially under highly acidic condition, negatively charged chromate ions ($HCrO_4^-$) binds to the positive surface of biochar through electrostatic attraction. The reduction of Cr(VI) to Cr(III) occurs on the biochar through redox process.

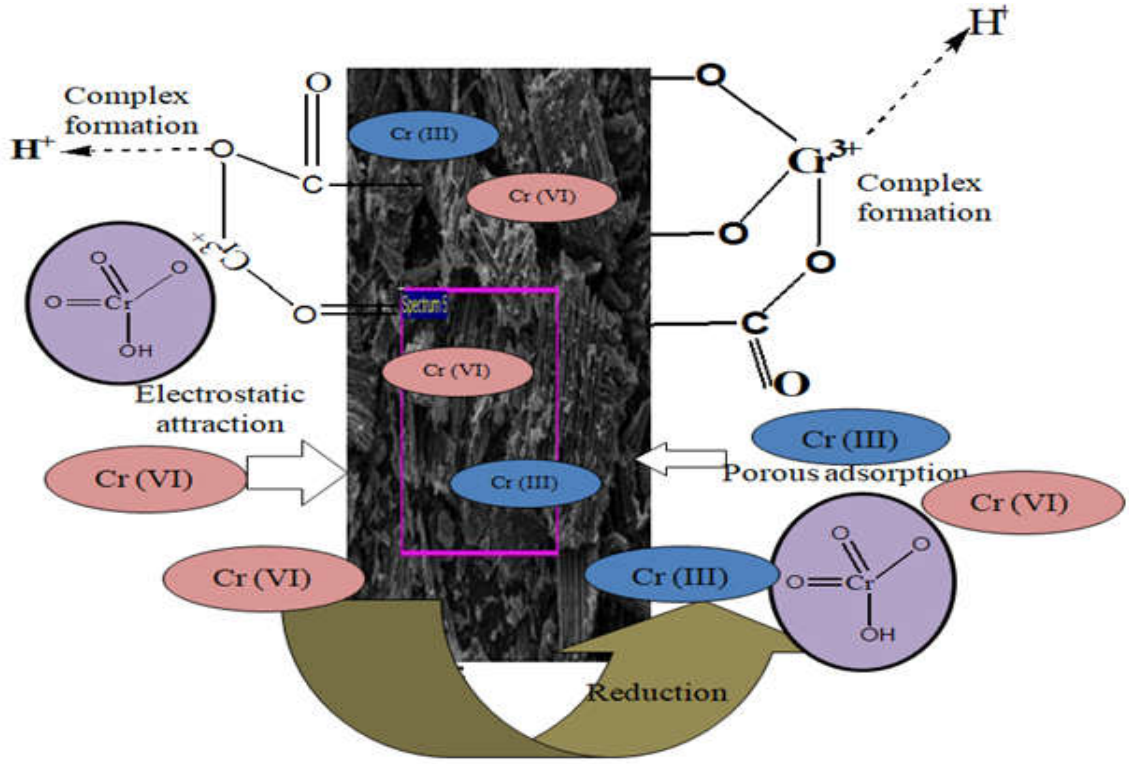

Fig. 6.19 Cr(VI) adsorption mechanism by SS biochar

The surface of biochar contains various functional groups like aldehydes (-CHO), ketones (C=O), carboxylic acids (-COOH) etc. which has the self-regulating ability to accept or release proton depending upon the change in external pH conditions. After Cr(VI) got adsorbed on the biochar surface, it was reduced to Cr(III) from the electron supplied from the O atom of phenol, alcohols. Further, the negatively charged carboxylic group on the biochar surface bound the Cr(III) onto it through complexation

or ion exchange (Chen et al., 2020). The presence of Cr(III) and Cr(VI) on biochar surface has been confirmed by XPS survey and shown in Fig. 6.6. Thus, this removal mechanism indicated that SS biochar can effectively reduce Cr(VI) to Cr(III) and also it can stabilize Cr(III) contained by the biochar surface which reduces secondary land pollution.

6.3.10 Regeneration study

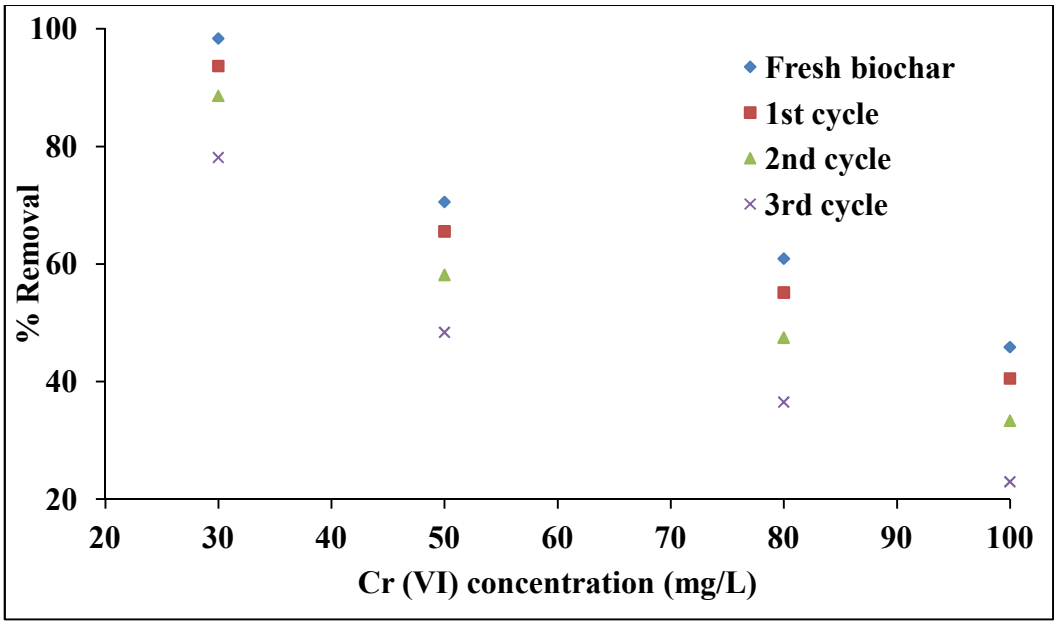

Fig. 6.20 Cr(VI) removal using fresh and regenerated biochar

The Cr(VI) loaded adsorbent is not always safe to dispose off directly to the atmosphere because of various environmental limitations and also it will promote secondary ground pollution as well. Thus, to evade such adversity, regeneration and reuse of the adsorbent is always a possible solution. In the present research, Cr(VI) laden biochar was regenerated and was reused for the removal of Cr(VI) in the concentration range from 30-100 mg/L. Since removal of Cr(VI) was favoured at lower pH, a solution with higher

pH can be used for the desorption process. Thus, in this study, Cr(VI) loaded biochar was eluted using 1 N NaOH for 24 h followed by washing with 1 N HCl. Further washing was done with double distilled water and then biochar was oven dried for further use. The regenerated biochar was then used for Cr(VI) removal for the next 3 cycles and the results are presented in Fig. 6.20. The regenerated biochar showed appreciable results and can be recommended for its reuse in Cr(VI) removal. It is also evident from Table 6.10 that SS biochar has more adsorption capacity as compare most of adsorbents used earlier.

Table 6.10 Comparison of adsorption capacity for different adsorbents

Adsorbents	pH (maximum removal)	Adsorption capacity (mg/g)	References
Bone char	1	8.41	(Hyder et al., 2015)
Pineapple peel derived biochar	2	7.44	(Wang et al., 2016)
Oak wood char	2	3.03	(Mohan et al., 2011)
Oak bark char	2	4.61	(Mohan et al., 2011)
Coconut shell activated carbon	2	9.53	(Mohan et al., 2005)
SS biochar	2	9.62	**This study**

6.4 Conclusion

The present study describes the effective utility of SS biochar for Cr(VI) removal from aqueous phase. Process variables like pH, initial Cr(VI) concentration and temperature were found to be influencing in removing Cr(VI) from aqueous phase. RSM envisaged optimum result at pH 2.07, temperature 30.72 °C and dose/Cr(VI) concentration 160.93 for achieving maximum removal with desirability of 1. The high value of F and low p-

value (< 0.0001) verified the significance of the model. ANOVA revealed high R^2 values (98.71 %) for Cr(VI) removal, suggestive of excellent accuracy of the quadratic model. Equilibrium was achieved in a short time of 60 min. FTIR study showed functional group like C-H, C=O, N-H, O-H, C-O, etc. were involved in the adsorption process and XPS analysis affirmed that the Cr(VI) is getting reduced to Cr(III). Langmuir isotherm gave best fit to the experimental data and Q_0 was found to be 9.62 mg/g at 30 °C with R^2 of 98.7 %. From kinetic point of view, second order rate equation showed better alignment as compare to first order model. Thermodynamic study exposed the process is both exothermic and spontaneous. Boyd model confirmed that film diffusion is the rate restrictive step in removing Cr(VI) using SS biochar. Comparing the removal efficiency and adsorption capacity with other adsorbents, SS biochar can be a competent adsorbent for treating wastewater containing Cr(VI).